Peter Frolkovič; Viera Kleinová
Two methods for optical flow estimation

TWO METHODS FOR OPTICAL FLOW ESTIMATION[*]

PETER FROLKOVIČ[†] AND VIERA KLEINOVÁ.

Abstract. In this paper we describe two methods for optical flow estimation between two images. Both methods are based on the backward tracking of characteristics for advection equation and the difference is on the choice of advection vector field. We present numerical experiments on 2D data of cell nucleus.

Key words. optical flow, advection equation, level-set motion, characteristic curves

AMS subject classifications. 35L45, 65M25, 68U10

1. Introduction. Optical flow is an important topic in various fields including computer vision and image processing. It is a technique that is based on estimating a deformation between images of video sequence.

The most popular methods for optical flow estimation are so-called differential methods [1, 2, 3, 4, 5, 9]. These methods are based on spatial derivatives of images. We are interested in two approaches.

The first approach is based on the method created by Lucas and Kanade [5] where it is assumed that the optical flow is constant locally within some neighborhood of each pixel in images. This approach is extended to a nonlocal form by e.g. Horn and Schunck [3] where the optical flow is estimated globally over entire image.

The second approach is based on level-set formulation [6] and it is directly motivated by models described by Sapiro et al. [1] and Vemuri et al. [9]. The methods are appropriate especially to estimate a non-rigid deformation when the objects in images change their shape.

The main goal of this paper is to apply both approaches with the backward tracking of characteristic curves for related advection equation to estimate the optical flow together with their numerical implementation. Moreover we show the results obtained by Lucas-Kanade method and the method based on level-set motion and we suggest their combination for some type of images.

2. Formulation of optical flow. Let us represent two images $F(\mathbf{x}) \in \mathbf{R}$ and $G(\mathbf{x}) \in \mathbf{R}$ by functions of intensity on a domain $\Omega \subset \mathbf{R}^2$ for $\mathbf{x} \in \Omega$ and $\mathbf{x} = (x, y)$. The main goal of optical flow estimation is to find a deformation $\vec{U}(\mathbf{x})$ between $F(\mathbf{x})$ and $G(\mathbf{x})$ such that $F(\mathbf{x} - \vec{U}(\mathbf{x})) = G(\mathbf{x})$.

The basic idea of our approach is to search for a function $f = f(\mathbf{x}, t)$ that fulfils the advection equation

$$(2.1) \qquad \partial_t f(\mathbf{x}, t) + \vec{u}(\mathbf{x}, t) \cdot \nabla f(\mathbf{x}, t) = 0, \qquad f(\mathbf{x}, 0) = F(\mathbf{x}),$$

for $t \in [0, T]$ where $T > 0$ and $\vec{u} = \vec{u}(\mathbf{x}, t) = (u(\mathbf{x}, t), v(\mathbf{x}, t))$ has to be specified such that $f(\mathbf{x}, T) = G(\mathbf{x})$.

[†]Department of Mathematics and Descriptive Geometry, Slovak University of Technology, Radlinského 11, 810 05 Bratislava, Slovakia (`peter.frolkovic@stuba.sk`).

Once the advection equation (2.1) is solved, the characteristic curves $X(\mathbf{x}, \tilde{t}; t)$ generated by $\vec{u}$ can be used that are obtained as solutions of ordinary differential equations

$$(2.2) \qquad \dot{X}(\mathbf{x}, \tilde{t}; t) = \vec{u}(X(\mathbf{x}, \tilde{t}; t), t), \qquad X(\mathbf{x}, \tilde{t}; \tilde{t}) = \mathbf{x},$$

for $\tilde{t} \in [0, T]$ and $\mathbf{x} \in \Omega$. The value $X(\mathbf{x}, \tilde{t}; t)$ is a position X of characteristic curve at time t such that the position at time $\tilde{t}$ is $\mathbf{x}$.

For the solution $f(\mathbf{x}, t)$ of advection equation (2.1) we see that the time derivative of $f(X(\mathbf{x}, \tilde{t}; t), t)$ vanishes along $X(\mathbf{x}, \tilde{t}; t)$,

$$\frac{\mathrm{d}}{\mathrm{d}t} f(X(\mathbf{x}, \tilde{t}; t), t) = \partial_t f(X(\mathbf{x}, \tilde{t}; t), t) + \dot{X}(\mathbf{x}, \tilde{t}; t) \cdot \nabla f(X(\mathbf{x}, \tilde{t}; t), t)$$
$$= \partial_t f(X(\mathbf{x}, \tilde{t}; t), t) + \vec{u}(X(\mathbf{x}, \tilde{t}; t), t) \cdot \nabla f(X(\mathbf{x}, \tilde{t}; t), t) = 0.$$

We can conclude that $f(\mathbf{x}, t)$ is constant along the characteristics.

In this paper we use the backward tracking of characteristics to compute the solution f of (2.1) by

$$(2.3) \qquad f(\mathbf{x}, \tilde{t}) = F(X(x, \tilde{t}; 0))$$

for $\tilde{t} > 0$. Consequently, the deformation $\vec{U}(\mathbf{x})$ is defined for $\tilde{t} = T$ by

$$(2.4) \qquad \vec{U}(\mathbf{x}) = \mathbf{x} - X(\mathbf{x}, T; 0).$$

Next we describe two methods how to obtain the vector field $\vec{u}$.

2.1. Lucas-Kanade method. The method belongs to local methods and it solves the advection equation (2.1) for unknowns $\vec{u} = (u, v)$ separately for each $\mathbf{x} \in \Omega$ and $t = 0, 1, \dots$. The solution is found starting with $t = 0$ by minimizing the function

$$(2.5) \qquad H(u, v) = W_\sigma * (\partial_x f u + \partial_y f v + \partial_t f)^2,$$

where $*$ denotes the convolution. Here W_σ is a weight function and it is usually set to a Gaussian of a standard deviation σ [5]. The minimum of $H(u, v)$ is reached if $\partial_u H(u, v) = 0$ and $\partial_v H(u, v) = 0$

$$0 = W_\sigma * [2(\partial_x f u + \partial_y f v + \partial_t f)\partial_x f],$$
$$0 = W_\sigma * [2(\partial_x f u + \partial_y f v + \partial_t f)\partial_y f].$$

The unknowns $(u(\mathbf{x}, t), v(\mathbf{x}, t))$ are obtained from the linear system in the form

$$(2.6) \quad \begin{pmatrix} W_\sigma * (\partial_x f)^2 & W_\sigma * (\partial_x f \partial_y f) \\ W_\sigma * (\partial_y f \partial_x f) & W_\sigma * (\partial_y f)^2 \end{pmatrix} \begin{pmatrix} u \\ v \end{pmatrix} = \begin{pmatrix} -W_\sigma * (\partial_x f \partial_t f) \\ -W_\sigma * (\partial_y f \partial_t f) \end{pmatrix}.$$

Once the vector field $\vec{u}$ is found for each $\mathbf{x} \in \Omega$, one can compute $f(\mathbf{x}, t+1)$ using (2.3) and the method can return to (2.5) to compute $\vec{u}(\mathbf{x}, t+1)$ and so on.

2.2. Method based on level-set motion. The method is motivated by Sapiro et al. [1] and Vemuri et al. [9]. In this case we consider $\vec{u}$ in the advection equation (2.1) of the form

$$(2.7) \qquad \vec{u}(\mathbf{x}, t) = \begin{cases} -S(\mathbf{x}, t) \frac{\nabla f(\mathbf{X}, t)}{|\nabla f(\mathbf{X}, t)|} & |\nabla f(\mathbf{x}, t)| \neq 0 \\ \vec{0} & |\nabla f(\mathbf{x}, t)| = 0, \end{cases}$$

where $S(\mathbf{x}, t)$ is a speed in normal direction, so the equation (2.1) can be rewritten in the form

$$(2.8) \qquad \partial_t f(\mathbf{x}, t) = S(\mathbf{x}, t)|\nabla f(\mathbf{x}, t)|, \qquad f(\mathbf{x}, 0) = F(\mathbf{x}).$$

The natural choice for the speed $S(\mathbf{x}, t)$ is

$$(2.9) \qquad S(\mathbf{x}, t) = \alpha(\mathbf{x}, t)(G(\mathbf{x}) - f(\mathbf{x}, t)),$$

where $\alpha(\mathbf{x}, t) > 0$ is a free parameter function that will be defined conveniently in numerical method later. Using (2.7) the advection equation (2.1), resp. (2.8), is solved directly for the unknown function f and $\vec{u}$ is determined from (2.7).

3. Numerical implementation. We assume 2D gray scale images with centers $\mathbf{x}_{ij} = (i, j)$ of pixels for $i = 0, \ldots, I - 1$ and $j = 0, \ldots, J - 1$. The distance between two centers $\mathbf{x}_{i+1j} - \mathbf{x}_{ij}$ and $\mathbf{x}_{ij+1} - \mathbf{x}_{ij}$ is 1 and the time points are chosen to be $t^n = n$ for $n = 0, 1, \ldots$. The images $F(\mathbf{x})$ and $G(\mathbf{x})$ for $\mathbf{x} \in \Omega$ are represented by bilinear interpolation of the discrete values of their intensities $F_{ij} = F(\mathbf{x}_{ij})$ and $G_{ij} = G(\mathbf{x}_{ij})$. The main goal of this paper is to approximate the deformation $\vec{U}(\mathbf{x})$ such that $G_{ij} \approx F(\mathbf{x}_{ij} - \vec{U}_{ij})$, where $\vec{U}_{ij} \approx \vec{U}(\mathbf{x}_{ij})$.

Once the vector field $\vec{u}$ is approximated by discrete values $\vec{u}_{ij}^n \approx \vec{u}(\mathbf{x}_{ij}, t^n)$, see later, the characteristic curves are approximated by $X_{ij}^{n,m} \approx X(\mathbf{x}_{ij}, t^n; t^m)$ at any time t^n by numerical approximation of (2.2) for $m = n - 1, \ldots, 0$, namely

$$(3.1) \qquad X_{ij}^{n,m} = X_{ij}^{n,m+1} - \vec{u}^m(X_{ij}^{n,m+1}), \qquad X_{ij}^{n,n} = \mathbf{x}_{ij},$$

where $\vec{u}^m(\mathbf{x})$ is the bilinear interpolation of discrete values $\vec{u}_{ij}^m$.

Consequently, we can approximate $f_{ij}^n \approx f(\mathbf{x}_{ij}, t^n)$ as in equation (2.3) by

$$(3.2) \qquad f_{ij}^n = F(X_{ij}^{n,0}) \approx F(X(\mathbf{x}_{ij}, t^n; 0)),$$

for $n > 0$ and for $n = 0$ we set $f_{ij}^0 = F_{ij}$.

When $n = N$ the deformation $\vec{U}(\mathbf{x})$ between $F(\mathbf{x})$ and $G(\mathbf{x})$ is given by

$$(3.3) \qquad \vec{U}_{ij} = \mathbf{x}_{ij} - X_{ij}^{N,0}.$$

The stopping time t^n for some $n = N$ is determined by estimating the distance between f_{ij}^n and G_{ij}.

3.1. Numerical implementation of Lucas-Kanade method. The numerical approximation of the linear system (2.6) is obtained by solving

$$(3.4) \qquad \begin{pmatrix} W_\sigma * (\partial_x f_{ij}^n)^2 & W_\sigma * (\partial_x f_{ij}^n \partial_y f_{ij}^n) \\ W_\sigma * (\partial_y f_{ij}^n \partial_x f_{ij}^n) & W_\sigma * (\partial_y f_{ij}^n)^2 \end{pmatrix} \begin{pmatrix} u_{ij}^n \\ v_{ij}^n \end{pmatrix} = \\ = \begin{pmatrix} -W_\sigma * (\partial_x f_{ij}^n \partial_t f_{ij}^n) \\ -W_\sigma * (\partial_y f_{ij}^n \partial_x f_{ij}^n) \end{pmatrix}.$$

where $u_{ij}^n \approx u(\mathbf{x}_{ij}, t^n)$ and $v_{ij}^n \approx v(\mathbf{x}_{ij}, t^n)$ and $\partial_t f_{ij}^n = (G_{ij} - f_{ij}^n)$. The spatial derivatives $\partial_x f_{ij}^n$ and $\partial_y f_{ij}^n$ are approximated by central differences

$$(3.5) \qquad \begin{aligned} \partial_x f_{ij}^n &= \frac{f_{i+1j}^n - f_{i-1j}^n}{2} \\ \partial_y f_{ij}^n &= \frac{f_{ij+1}^n - f_{ij-1}^n}{2}. \end{aligned}$$

The discrete convolution with Gaussian function W_σ is defined as follows

$$(3.6) \qquad W_\sigma * f(x,y,t) = \frac{1}{\sum_{i,j} w_{ij}} \sum_{i,j} w_{ij} f(x+i, y+j, t) \,,$$

where $-3\sigma < i < 3\sigma$ and $-3\sigma < j < 3\sigma$ and

$$(3.7) \qquad w_{ij} = \frac{1}{2\pi\sigma^2} \exp^{-\frac{i^2 + j^2}{2\sigma^2}} \,,$$

where σ is a standard deviation that must be chosen by users. To do so we choose a convolution matrix with the elements w_{ij} to have a size $E \times E$ where E is an odd integer and $\sigma = E/6$. The dimension E determines the neighborhood of each pixel for which the assumption about constant optical flow is considered. A proper choice of E, respectively σ, is a nontrivial requirement of the original Lucas-Kanade method. Later for some numerical experiments we discuss a proper guess of σ and an influence of different choices on results.

Once the approximations $\vec{u}_{ij}^m$ are available, we can compute f_{ij}^{n+1} by using (3.2) and proceed to next time step.

3.2. Numerical implementation of the method based on level-set motion. Formally, we can approximate (2.8) by a numerical scheme

$$(3.8) \qquad \tilde{f}_{ij}^{n+1} = f_{ij}^n + S_{ij}^n |\nabla f_{ij}^n|$$

where $S_{ij}^n = \alpha_{ij}^n (G_{ij} - f_{ij}^n) \approx S(\mathbf{x}_{ij}, t^n)$. To do so we approximate firstly the gradient ∇f_{ij}^n in (3.8) using the Rouy-Tourin scheme [8]

$$(3.9) \qquad \partial_x f_{ij}^n = \begin{cases} f_{ij}^n - f_{i-1j}^n & f_{i-1j}^n = \text{ext}\{f_{i-1j}^n, f_{ij}^n, f_{i+1j}^n\} \\ f_{i+1j}^n - f_{ij}^n & f_{i+1j}^n = \text{ext}\{f_{i-1j}^n, f_{ij}^n, f_{i+1j}^n\} \\ 0 & f_{ij}^n = \text{ext}\{f_{i-1j}^n, f_{ij}^n, f_{i+1j}^n\} \end{cases}$$

$$(3.10) \qquad \partial_y f_{ij}^n = \begin{cases} f_{ij}^n - f_{ij-1}^n & f_{ij-1}^n = \text{ext}\{f_{ij-1}^n, f_{ij}^n, f_{ij+1}^n\} \\ f_{ij+1}^n - f_{ij}^n & f_{ij+1}^n = \text{ext}\{f_{ij-1}^n, f_{ij}^n, f_{ij+1}^n\} \\ 0 & f_{ij}^n = \text{ext}\{f_{ij-1}^n, f_{ij}^n, f_{ij+1}^n\} \end{cases}$$

where ext denotes a minimum or maximum with the choice

$$(3.11) \qquad \text{ext} = \begin{cases} \min & S_{ij}^n < 0 \\ \max & S_{ij}^n > 0 \,. \end{cases}$$

Secondly we have to define the values $\alpha_{ij}^n \approx \alpha(\mathbf{x}_{ij}, t^n) > 0$ to compute S_{ij}^n in (3.8). We propose to choose maximal values of α_{ij}^n to speed up the computation such that the so called CFL condition [7] and some stopping criteria are fulfilled, namely

$$(3.12) \qquad \alpha_{ij}^n = \min\left(\frac{1}{|\nabla f_{ij}^n| + \epsilon}, \frac{|\nabla f_{ij}^n|}{|G_{ij} - f_{ij}^n|(|\partial_x f_{ij}^n| + |\partial_y f_{ij}^n| + \epsilon)} \right) ,$$

where $\epsilon > 0$ is a small number to avoid a division by zero. The parameter ϵ is set to 10^{-8} for all presented numerical experiments, and different choices, e.g. $= 10^{-4} \leq \epsilon \leq= 10^{-8}$, have no visible influence on the results.

Once the approximations in the right hand side of (3.8) are available then the values $\vec{u}_{ij}^n$ are computed by approximation of (2.7)

$$(3.13) \qquad \vec{u}_{ij}^n = \begin{cases} -S_{ij}^n \dfrac{\nabla f_{ij}^n}{|\nabla f_{ij}^n|} & |\nabla f_{ij}^n| \neq 0 \\ \vec{0} & |\nabla f_{ij}^n| = 0 , \end{cases}$$

and the scheme (3.2) can be used to compute f_{ij}^{n+1}.

4. Experimental results. We present the results obtained from images of cell nucleus of zebrafish, see Fig. 4.1, Fig. 4.5 and Fig. 4.8. The images were preprocessed using a segmentation of the cell nucleus. The data are originally three dimensional, but we consider only two dimensional images. Some images contain a large deformation so they are quite challenging for the optical flow estimation.

Once an estimation of $\vec{U}(\mathbf{x})$ is obtained, we determine the approximation of image $F(x - \vec{U}(\mathbf{x}))$ to check the approximation quality of numerical methods by comparing it with the original image $G(\mathbf{x})$. Namely the difference image $|G(\mathbf{x}) - F(\mathbf{x} - \vec{U}(\mathbf{x}))|$ is shown that should be white if there is no error in the approximation. The optical flow is presented graphically as $-\vec{U}(\mathbf{x})$, because we want to show from where does the position $\mathbf{x}$ in the image $G(\mathbf{x})$ comes from the image $F(\mathbf{x} - \vec{U}(\mathbf{x}))$. For a clarity, we present every fifth vector component of the optical flow in figures.

4.1. Cell movement. The first experiment includes the movement of cell nucleus. The input images are shown in Fig. 4.1 and the cell simply moves from the left to the right. The image size is 250×250.
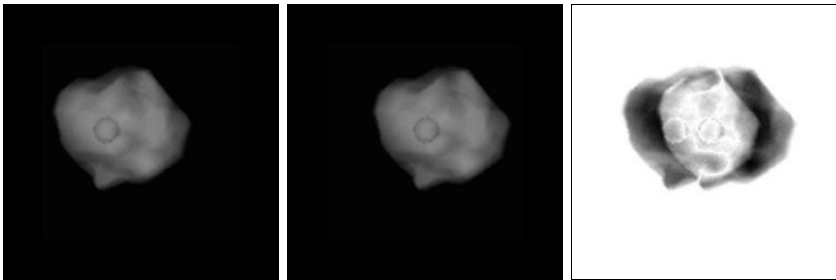

FIG. 4.1. *The input images of cell movement. From the left to the right: the first image $F(\boldsymbol{x})$, the second image $G(\boldsymbol{x})$, the difference image $|G(\boldsymbol{x}) - F(\boldsymbol{x})|$.*

Firstly, Lucas-Kanade method is used with the discrete convolution matrix of dimension 201×201 using the standard deviation $\sigma = 33.5$. In Fig. 4.2 (right) we can see a well resolved constant optical flow for this choice of σ. This size of convolution matrix was guessed from the size of a deformation caused by the optical flow visible in the difference image $|G(x) - F(x)|$.

We present computations also with a too small value of σ. In Fig. 4.3 the results of Lucas-Kanade method with standard deviation $\sigma = 16.83$ are shown when the discrete convolution matrix of the dimension 101×101 is used. From the visual inspection of optical flow in Fig. 4.3 (right) and difference image in Fig. 4.3 (middle) we can see that such convolution is not appropriate and the results are far away from expected ones.

Next we estimate the optical flow based on the level set motion. The results are presented in Fig. 4.4. The difference image in Fig. 4.4 (middle) shows that the result

is satisfactory. In Fig. 4.4 (right) we can see the obtained optical flow in normal direction that is not suitable for a visualization of movement by a constant vector field.
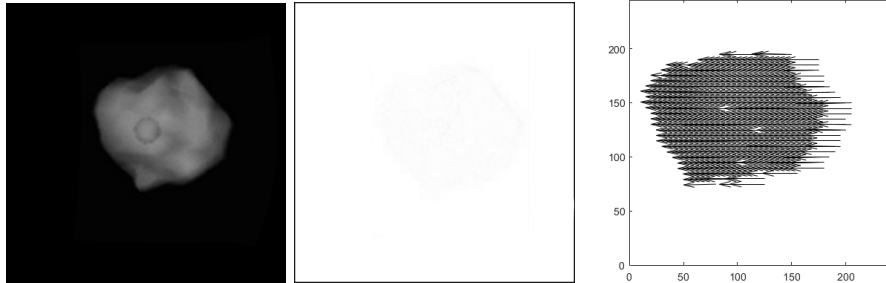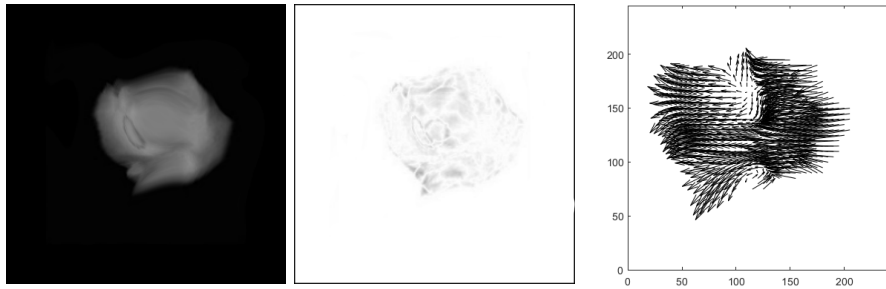

FIG. 4.2. *The results obtained by Lucas-Kanade method with* $\sigma = 33.5$. *From the left to the right: the image* $F(x - \vec{U}(x))$, *the difference image* $|G(\boldsymbol{x}) - F(\boldsymbol{x} - \vec{U}(\boldsymbol{x}))|$, *the optical flow* $-\vec{U}(\boldsymbol{x})$.

FIG. 4.3. *The results obtained by Lucas-Kanade method with* $\sigma = 16.83$. *From the left to the right: the image* $F(x - \vec{U}(x))$, *the difference image* $|G(\boldsymbol{x}) - F(\boldsymbol{x} - \vec{U}(\boldsymbol{x}))|$, *the optical flow* $-\vec{U}(\boldsymbol{x})$.

FIG. 4.4. *The results obtained by the method based on level set motion. From the left to the right: the image* $F(x - \vec{U}(x))$, *the difference image* $|G(\boldsymbol{x}) - F(\boldsymbol{x} - \vec{U}(\boldsymbol{x}))|$, *the optical flow* $-\vec{U}(\boldsymbol{x})$.

4.2. Cell deformation. In the second experiment the images in Fig. 4.5 represent a change of cell shape. The image size is 300×300.

The results are shown in Fig. 4.6 for Lucas-Kanade method and in Fig. 4.7 for method based on level set motion.

For Lucas-Kanade method the matrix of dimension 201×201 with $\sigma = 33.5$ is used as in the previous example. The optical flow in Fig. 4.6 (right) is smooth, but
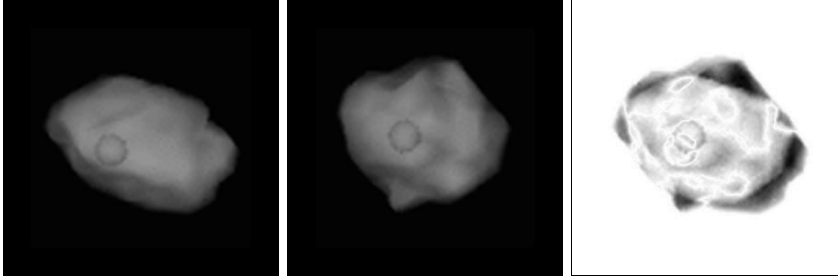
FIG. 4.5. *The input images of the deformation of cell. From the left to the right: the first image $F(x)$, the second image $G(\boldsymbol{x})$, the difference image $|G(\boldsymbol{x}) - F(\boldsymbol{x})|$.*

from the visual inspection of difference image in Fig. 4.6 (middle) we can see that this method can not change the shape of cell properly.

The difference image in Fig. 4.7 (middle) and the image after applying the optical flow in Fig. 4.7 (left) show us that the results are satisfactory.

FIG. 4.6. *The results obtained by Lucas-Kanade method with $\sigma = 33.5$. From the left to the right: the image $F(x - \vec{U}(\boldsymbol{x}))$, the difference image $|G(\boldsymbol{x}) - F(x - \vec{U}(\boldsymbol{x}))|$, the optical flow $-\vec{U}(\boldsymbol{x})$.*
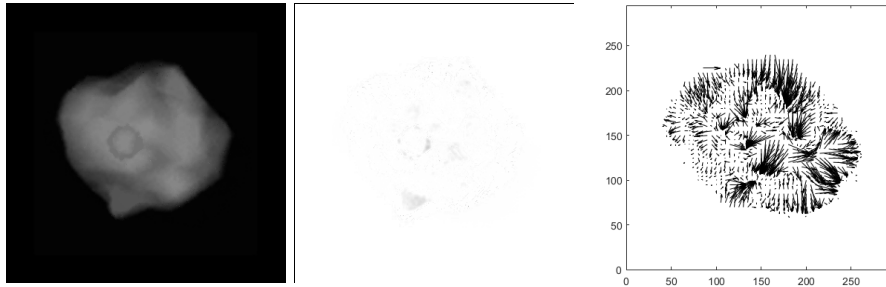

FIG. 4.7. *The results obtained by the method based on level-set motion. From the left to the right: the image $F(x - \vec{U}(\boldsymbol{x}))$, the difference image $|G(\boldsymbol{x}) - F(x - \vec{U}(\boldsymbol{x}))|$, the optical flow $-\vec{U}(\boldsymbol{x})$.*

4.3. Movement and deformation of cells. The last experiment include the motion and deformation of four cells. The input images are shown in Fig. 4.8. The size of images is 640×600.

In this case we present the results obtained by combining the Lucas-Kanade method and the method based on level-set motion.
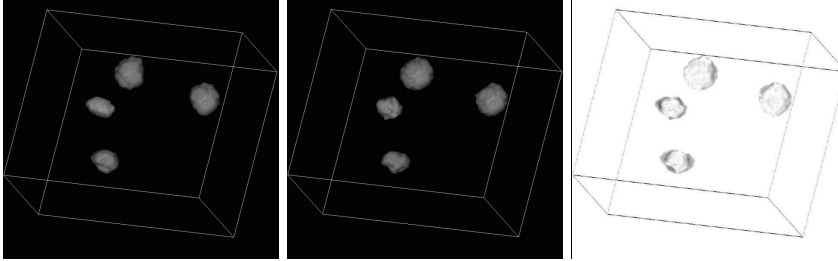

FIG. 4.8. *The input images of movement and deformation of the cells. Form left to right: the first image $F(\boldsymbol{x})$, the second image $G(\boldsymbol{x})$, the difference image $|G(\boldsymbol{x}) - F(\boldsymbol{x})|$.*

Firstly, we estimate the optical flow using the Lucas-Kanade method. The standard deviation is chosen $\sigma = 8.5$ as the deformation by the optical flow has a smaller size than in the previous examples. The resulting optical flow is shown in Fig. 4.9 (right). For a better visualisation the zooms of the optical flow in Fig. 4.9 (right) are presented for each cell in Fig. 4.10.

From the visual inspection of difference image $|G(x) - F(x - \vec{U}(x))|$ in Fig. 4.9 (middle) we can see that the results are not satisfactory as the method can move the cells but it does not change their shapes properly. This can be seen from the difference image and also from the obtained image in Fig. 4.9 (left).
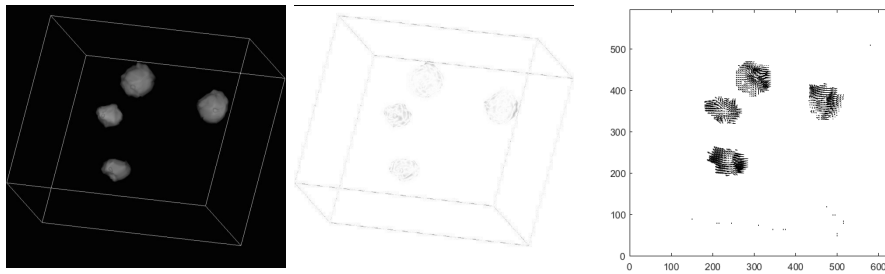

FIG. 4.9. *The results obtained by Lucas-Kanade method with $\sigma = 8.5$. From the left to the right: the image $F(x - \vec{U}(\boldsymbol{x}))$, the difference image $|G(\boldsymbol{x}) - F(\boldsymbol{x} - \vec{U}(\boldsymbol{x}))|$, the optical flow $-\vec{U}(\boldsymbol{x})$.*
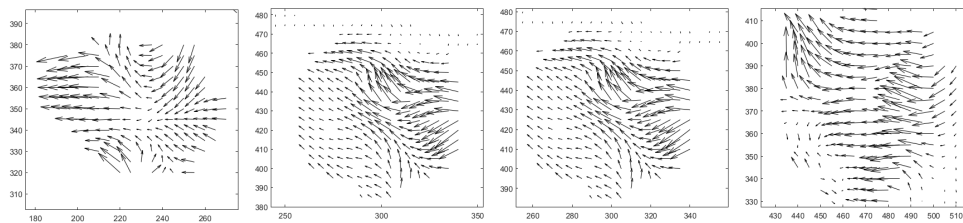

FIG. 4.10. *Zooms of the optical flow obtained by Lucas-Kanade method.*

The next step is to apply the method based on level-set motion on the obtained image from Lucas-Kanade method and to compute the total optical flow.

The results after applying two methods is shown in Fig. 4.11. Again we present the zooms of optical flow for each cells in Fig. 4.12. From the visual inspection of the difference image and image after applying optical flow in Fig. 4.11 we can see, that the results of Lucas-Kanade method were improved by the correction of method based on level set motion.
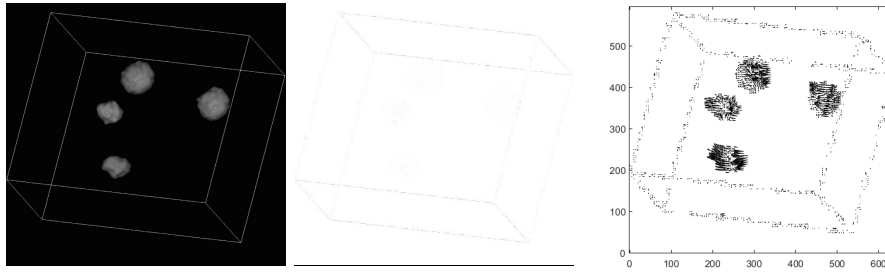

FIG. 4.11. *The results obtained by method based on level-set motion after Lucas-Kanade method. From the left to the right: the image $F(x - \vec{U}(x))$, the difference image $|G(x) - F(x - \vec{U}(x))|$, the optical flow $-\vec{U}(\boldsymbol{x})$.*
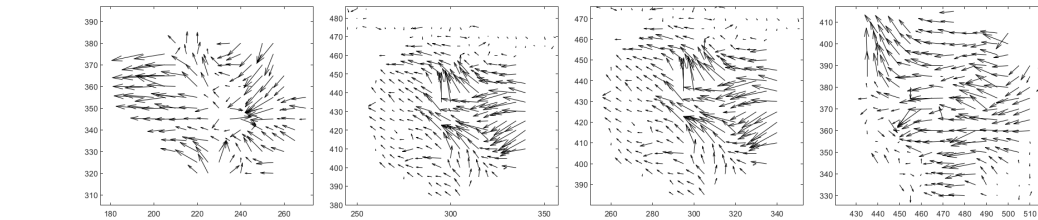

FIG. 4.12. *Zooms of the total optical flow.*

5. Conclusions. In this work we present two methods to estimate the optical flow using the backward tracking of characteristics based on two standard approaches. To study which approach is more suitable for which type of optical flow estimation we present numerical experiments and discuss the results. The Lucas-Kanade method [5] assumes that the optical flow does not vary too much in a neighborhood of each pixel when the size of such neighborhood must be set by the dimension of convolution matrix. The method gives best results when the vector field of optical flow is almost constant. The method based on the level set motion [1, 9] does not require such assumption as it estimates only the deformation by optical flow in the normal direction to isolines of image. It is appropriate when no translation is given by the optical flow and only a shape deformation can be observed between two images. In this work we present preliminary results when these two methods are combined to obtain more appropriate optical flow estimation.

REFERENCES

[1] M. Bartalmío, G. Sapiro and G. Randall, *Morphing Active Contours.*, IEEE Trans. PAMI, 22(7) (2000), pp. 733–737.

[2] A. Bruhn, J. Weickert, Ch. Schnrr, *Lucas/Kanade Meets Horn/Schunck: Combining Local and Global Optic Flow Methods.*, Int. Journal of Comp. Vision. , 61(3) (2005), pp. 211-231

[3] B. Horn, B. Schunck, *Determining optic flow.*, Artificial Intelligence, 17(1-3) (1981), pp. 185-203.

[4] V. Kleinová, *Algoritmy extrakcie rýchlostného poľa z postupnosti obrazov.*, Diploma thesis, Faculty of Civil Engineering, Slovak University of Technology in Bratislava (2014).

[5] B. Lucas, T. Kanade, *An iterative image registration technique with an application to stereovision.*, In Int. Joint Conf. on Artificial Intel, 2 (1981), pp. 674-679.

[6] S. Osher, J.A. Sethian, *Fronts Propagating with Curvature Dependent Speed: Algorithms Based on Hamilton-Jacobi Formulations* , J. Computational Physics, 79 (1988), pp. 12-49.

[7] R. J. LeVeque, *Finite Volume Methods for Hyperbolic Problems.*, Cambridge University Press, 1 (2002), ISBN: 0521009243.

[8] E. Rouy, A. Tourin, *A viscosity solutions approach to shape-from-shading.*, SIAM J. Num. Anal., 29 (1992), pp. 867-884.

[9] B.C. Vemuri, J. Ye, Y. Chen, C.M. Leonard, *Image registration via level-set motion: Applications to atlas-based segmentation.*, Medical Image Analysis, 7(1) (2003), pp. 1-20.